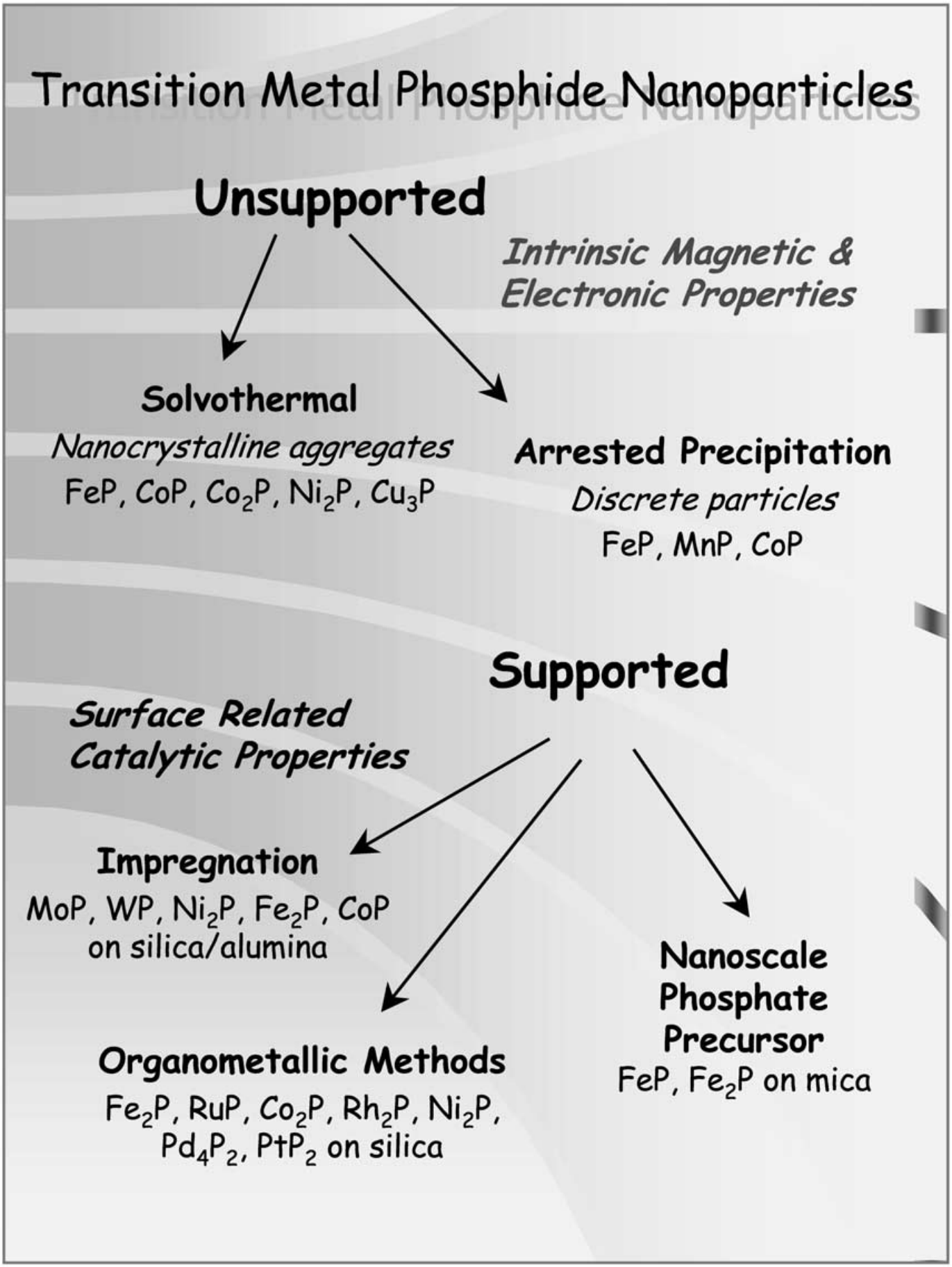

DOI: 10.1002/chem.200305775

Chemical Routes for Production of Transition-Metal Phosphides on the Nanoscale: Implications for Advanced Magnetic and Catalytic Materials

Stephanie L. Brock,* Susanthri C. Perera, and Kimber L. Stamm[a]

Abstract: Nanoparticulate transition-metal phosphides remain an unexplored, though emerging area of interest on the materials landscape, due principally to their promising magnetic and catalytic properties. This review describes synthetic strategies for the formation of both supported and unsupported transition-metal phosphide nanoparticles, provides a summary of their relevant magnetic and catalytic properties, and indicates new directions for exploration.

Keywords: heterogeneous catalysis · magnetic properties · nanostructures · phosphides · synthesis design

Introduction

The advance of nanotechnology is predicated on our ability to create and organize matter on length scales of 1–100 nm. However, despite significant advances in synthetic methodologies, the chemical complexity that can be achieved on the nanoscale, in terms of range of elements and compositions, is still relatively primitive. One class of compounds for which very few preparative methods have been explored is the transition-metal phosphides. These materials represent a synthetic challenge, as they can adopt a wide range of stoichiometries and structures. Additionally, phosphide sources tend to be very reactive, necessitating the use of rigorous air sensitive techniques. The impetus for meeting these challenges lies in the host of novel properties exhibited in bulk transition-metal phosphides, and the promise of unique, size-tunable properties in nanoscale phases. Of particular note in this review is the high catalytic activity for hydroprocessing of fuels, and the unique magnetic properties, which have implications for diluted magnetic semiconductor devices.

[a] Prof. S. L. Brock, Dr. S. C. Perera, K. L. Stamm
Department of Chemistry, Wayne State University
5101 Cass Avenue, Detroit, MI 48202 (USA)
Fax: (+1) 313-577-3102
E-mail: sbrock@chem.wayne.edu

This article will provide an overview of the various chemical methods (excluding physical routes, such as ball milling and molecular beam epitaxy) by which nanocrystalline transition-metal phosphides have been produced. These can be broken up into two categories: unsupported and supported particles. Research on the former is concerned with general synthetic methodology development and/or magnetic materials, whereas supported systems are largely of interest for their catalytic function. The influence of the nanoscale dimensions on the resultant physical properties will be discussed and new opportunities in this emerging area presented.

Unsupported Transition-Metal Phosphide Nanoparticles

State of the science—the solvothermal approach: The solvothermal approach is the most common reported method for the preparation of nanocrystalline transition-metal phosphides (Table 1). These reactions are conducted at temperatures above the normal boiling point of the solvent and at a pressure above normal atmospheric, typically in a sealed vessel (autogeneous pressure). Such *Chimie Douce* methods are ideal for producing metastable phases (as, in this case, nanoparticles), since the reactions take place at relatively low temperatures ($<250\,^{\circ}C$).[1]

The original methodology, reported first in 1997 by Qian and co-workers, involved reaction of sodium phosphide with transition-metal salts in benzene or toluene in a teflon-lined autoclave at temperatures of 150–190 °C.[2] This route was successfully applied to CoP/Co_2P,[2] Ni_2P,[3] and FeP.[4] Subsequently, the Qian group showed that white phosphorous (P_4) could also be used as a phosphide source in solutions of ammonium hydroxide or ethylene diamine. This permitted single phase Co_2P, Ni_2P, and Cu_3P to be formed.[5,6] Crystallite sizes range from 1–200 nm, depending on the reaction, but in all cases there appears to be a large (though frequently unreported) polydispersity. Although the authors postulate mechanisms for nanoparticle production and the role of various agents in particle formation and shape generation, there is still much that is not understood, including how the

 DOI: 10.1002/chem.200305775

Table 1. Summary of solvothermal methods for production of transition-metal phosphide nanoparticles.

Phase	Conditions and Comments	Average Crystallite Size (Determination Method) and Morphology	Ref.
FeP	$Na_3P/FeCl_3$ in benzene, 180–190 °C/24 h	~200 nm (TEM) non-uniform aggregates	[4]
CoP/ Co_2P	$Na_3P/CoCl_2$ in benzene, 150 °C/8 h; product is mixed phase	~25 nm (XRD) for CoP; spindle-shaped aggregates; ~49 nm (XRD) for Co_2P; spherical aggregates	[2]
Co_2P	$P_4/CoCl_2$ in en, 80–140 °C/12 h	~50 nm (TEM); plate-like aggregates	[5]
Ni_2P	$Na_3P/NiCl_2$ in toluene, 150 °C/8 h	10 nm (XRD); 1–20 nm, ave. 8–12 nm (TEM); spheres	[3]
	$P_4/NiCl_2$ in NH_4OH, 160 °C/12 h	16 nm (XRD); 28 nm (TEM); spherical aggregates	[6]
	$P_4/NiCl_2$ in en, 80–140 °C/12 h	50 nm (TEM); plate-like aggregates	[5]
	red P/$NiCl_2$ in en/polyacrylamide, 120–180 °C/20 h	20 nm (TEM, 180 °C) 200 nm (TEM, 120 °C); spherical aggregates	[7]
Cu_3P	$P_4/CuCl_2$ in NH_4OH, 140 °C/10 h	~26 nm (XRD); 24–40 nm, ave. 30 nm (TEM); plate-like aggregates	[6]
	$P_4/CuCl_2$ in en, 80–140 °C/12 h	~30–90 nm (TEM); spherical aggregates	[5]

particular phase and crystallite size can be controlled. Another drawback is the need for highly reactive phosphide sources (i.e., Na_3P or P_4). Furthermore, by the solvothermal pathway, nanoparticles are produced as insoluble aggregates, thus making size/physical-property evaluation difficult in these materials (indeed, no physical properties have been reported).

Very recently, there have been some promising results that suggest that a number of these hurdles can be overcome. In 2003, Qian and co-workers reported that red phosphorus can be used to produce nanocrystalline Ni_2P, although an acrylamide surfactant is needed to obtain success.[7] Additionally, other groups have shown that surfactant-aided solvothermal routes can be an effective way of controlling shape in nanoparticles of MoS_2[8] and CdS.[9] Appropriate modification of these synthetic routes can be expected to lead to better control of size and shape for transition-metal phosphide nanoparticles as well.

Arrested precipitation reactions with organometallic precursors—a fresh approach: In an effort to develop a route for the preparation of transition-metal phosphide nanoparticles that would be able to address concerns of particle size, solubility, shape, phase, and polydispersity, we have focused our attention on organometallic decomposition pathways. These methods are well developed for main-group-metal phosphides (i.e., InP, GaP)[10–14] and frequently involve reaction of the highly reactive phosphine, tris(trimethylsilyl)phosphine, with metal salts or complexes in the presence of a coordinating solvent [Eq. (1)].[15–17] Solvents include trioctylphosphine oxide (TOPO) or trioctylphosphine (TOP), which act to prevent aggregation of nucleating phosphide particles by coordinating to the surface of the growing particle. These solvents have high boiling points, therefore permitting reactions to be conducted at temperatures up to 350 °C (TOPO) to enhance crystallinity in the nanoparticles. Additionally, since TOP and TOPO bind tightly to the surface of the nanoparticles, they also have the added benefit of conferring solubility on the nanoparticles in nonpolar solvents, consequently facilitating isolation. Thus, appropriate control of temperature, time, and co-surfactants can result in highly soluble nanoparticles with low polydispersity and with good control of particle size and shape.[15–18] We reasoned this method should be equally amenable to transition-metal phosphides, with the added benefit that there would be phase control inherent in the reaction, since this procedure is formally nonredox. This is important for transition metals, since they can easily adopt a wide range of oxidation states and stoichiometries when combined with phosphorous, in contrast to their main group congeners.

$$MX_3 + P(SiMe_3)_3 \rightarrow MP + 3\,XSiMe_3 \quad (1)$$

We initiated our investigation with a study of iron and manganese phosphides, since these phases have a wide range of stoichiometries and associated magnetic properties of interest (Table 2). Nanocrystalline iron phosphides are implicated in the soft ferromagnetic properties associated with the alloy Ferrophos,[19] whereas nanocrystalline MnP precipitates have been found to form in Mn-doped InP,[20] and may, therefore, be a contributor to the ferromagnetism observed in a number of reported Mn-doped diluted magnetic semiconductors (e.g., Mn-doped $CdGeP_2$).[21–23]

Table 2. Structures and physical properties of selected phosphides of iron and manganese.

Phase	Structure-type	Electronic and Magnetic Properties	Ref.
Fe_3P	Fe_3P ($D0_c$)	metallic, ferromagnetic ($T_c = 716$ K)	[27]
Fe_2P	Fe_2P (C22)	metallic, ferromagnetic ($T_c = 266$ K)	[27]
FeP	MnP (B31)	metallic, helimagnetic ($T_N = 120$ K)	[27–29, 48]
FeP_2	Marcasite (C18)	semiconducting, ($E_g = 0.37$ eV) paramagnetic	[27]
MnP	MnP (B31)	metallic, ferromagnetic ($T_c = 291$ K); helimagnetic ($T_N \sim 50$ K)	[27, 30, 31]

Our initial reactions of [Fe(acac)$_3$] with $P(SiMe_3)_3$ in TOPO invariably led to a black, largely amorphous precipitate with only a small amount of pyridine-soluble colloid.[24] We soon found that co-surfactants such as dodecylamine (DA) or myristic acid (MA) are essential to moderate the reactivity, thus resulting in a high yield (85 % based on iron consumption) of soluble colloid.[25] Consistent with our assumptions about redox-neutral reactions, the powder X-ray diffraction (PXRD) pattern revealed that the likely product was nanocrystalline FeP (Figure 1 a). Furthermore, transmission electron microscopy (TEM) indicated that, in contrast

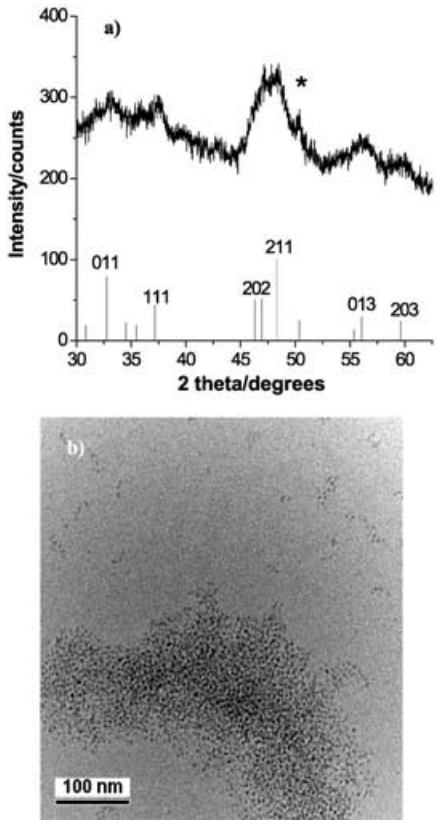

Figure 1. a) Powder X-ray diffraction spectrum of FeP nanoparticles prepared using Fe/dodecylamine (1:1 mol) at 260 °C. The line diagram illustrates the positions and relative intensities for reflections of FeP (JCPDS 39-0809), with major reflections indexed. The * denotes a background peak from the sample holder. b) Corresponding TEM micrograph (× 40 K); average particle size for FeP = 4.65 ± 0.74 nm (N = 425). Reproduced with permission from *Chem. Mater.* **2003**, *15*, 4034–4038. Copyright 2003 Am. Chem. Soc.

to the solvothermal method, discrete spherical nanoparticles (ca. 5 nm) can be produced with a low polydispersity (Figure 1 b). Interestingly, similar reactions with $[Mn(acac)_3]$ proved unfruitful. Although a clear change in solution color occurred upon annealing with $P(SiMe_3)_3$ in TOPO, it was never possible to isolate a product from this solution.

The ability to selectively form FeP led us to investigate whether we could similarly target the more metal-rich iron phosphide Fe_2P. However, according to the redox-neutral strategy, an unlikely iron precursor oxidation state of +1.5 would be required. Thus, we sought to test if mixing zerovalent and trivalent precursors in appropriate stoichiometry would permit access to nanocrystalline Fe_2P, according to Equation (2).

$$[Fe(acac)_3] + [Fe(CO)_5] + P(SiMe_3)_3 \rightarrow Fe_2P \quad (2)$$

Stoichiometric reactions of $[Fe(acac)_3]$ with $[Fe(CO)_5]$ and $P(SiMe_3)_3$ in TOPO produced FeP nanoparticles as the only crystalline product. In order to determine whether $[Fe(CO)_5]$ played a role in FeP production we subsequently explored reactions of $[Fe(CO)_5]$ with $P(SiMe_3)_3$. Once again, FeP nanoparticles were produced, suggesting that in addition to serving as a phosphide source, $P(SiMe_3)_3$ may also function as an oxidant.[26] Although the mechanism for this chemistry remains unclear, this strongly implies that "redox neutrality" does not hold for reactions between iron precursors and phosphines, but rather that there is a thermodynamic drive towards FeP.

This "redox active" route, then, provides an alternate pathway to explore for MnP nanoparticle formation. Indeed, treatment of $[Mn_2(CO)_{10}]$ with $P(SiMe_3)_3$ in TOPO with suitable co-surfactants leads to well-formed, crystalline MnP spherical nanoparticles of size 5–7 nm (depending on temperature) and low standard deviations (5–10 %) (Figure 2).[26] Furthermore, preliminary evidence suggests this method is equally amenable to CoP.[26]

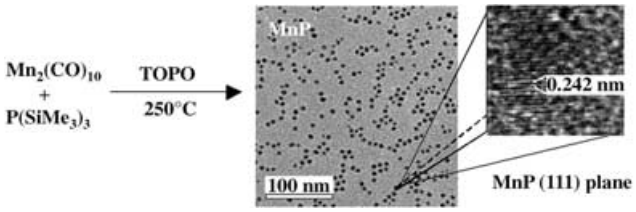

Figure 2. Synthetic scheme for production of MnP nanoparticles and associated TEM micrographs. Average particle size = 6.67 ± 0.33 nm. The lattice spacing visible in high resolution images (0.242 nm) corresponds to the (111) plane of MnP. Reproduced with permission from *J. Am. Chem. Soc.* **2003**, *125*, 13960–13961. Copyright 2003 Am. Chem. Soc.

Despite the ability to prepare FeP and MnP nanoparticles with excellent solubility and size control, these reactions still suffer from the drawback of requiring the highly reactive (and expensive) $P(SiMe_3)_3$ reagent. We wondered if more conventional phosphines would also yield the desired products. Specifically, we explored using trioctylphosphine (TOP) as both a phosphine source and a coordinating solvent and discovered that nanocrystalline MnP and FeP can be prepared equally well by the reaction of appropriate metal carbonyls with TOP. Indeed, under some conditions we even have access to unusual shapes, including rods and cubes. Importantly, this discovery provides an alternate strategy for targeting arsenides (e.g., MnAs) that precludes the use of $As(SiMe_3)_3$, which is not only toxic and pyrophoric, but not commercially available. These studies represent a current focus of research in our group.

Magnetic properties of FeP and MnP: For the first time, we have investigated the magnetic properties of FeP and MnP as function of crystallite size.[25,26] As bulk phases, both crystallize in the MnP structure type,[27] and both demonstrate a complex low-temperature magnetic structure (helimagnet) with net antiferromagnetic interactions, and a magnetic unit cell dimension of ~28 Å along the helical propagation axis.[28–31] For FeP, the transition occurs at 125 K, above which FeP is a paramagnet, whereas for MnP, the transition occurs at 50 K, and MnP is ferromagnetic above this temperature up until the Curie temperature (T_c = 291 K).

From magnetic susceptibility measurements on nanocrystalline FeP and MnP, we find that in both cases the transition to a helimagnetic state is completely shut down in the nanoparticles.[25,26] We attribute this to the fact that the nanoparticle dimension (4–8 nm) is approaching that of the magnetic unit cell for the helimagnetic configuration, thereby destabilizing this state. The consequence is that nanoparticulate FeP appears to be paramagnetic over the entire temperature range studied (300–5 K, Figure 3), whereas

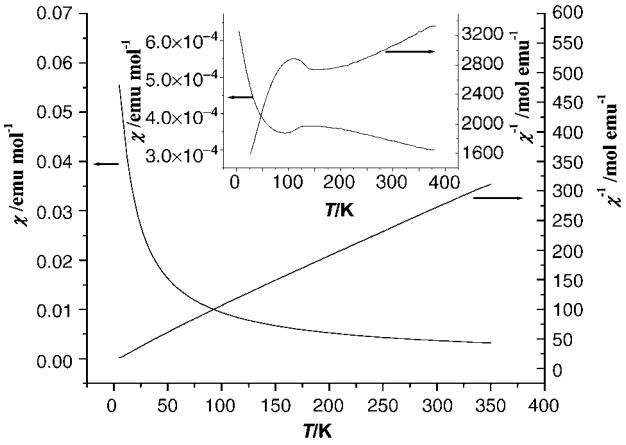

Figure 3. Temperature dependence of molar susceptibility (χ) and inverse molar susceptibility (χ^{-1}) for 4.7(7) nm FeP nanoparticles synthesized at 260 °C, and bulk FeP (inset), for $H = 3.0$ T. Reproduced with permission from *Chem. Mater.* **2003**, *15*, 4034–4038. Copyright 2003 Am. Chem. Soc.

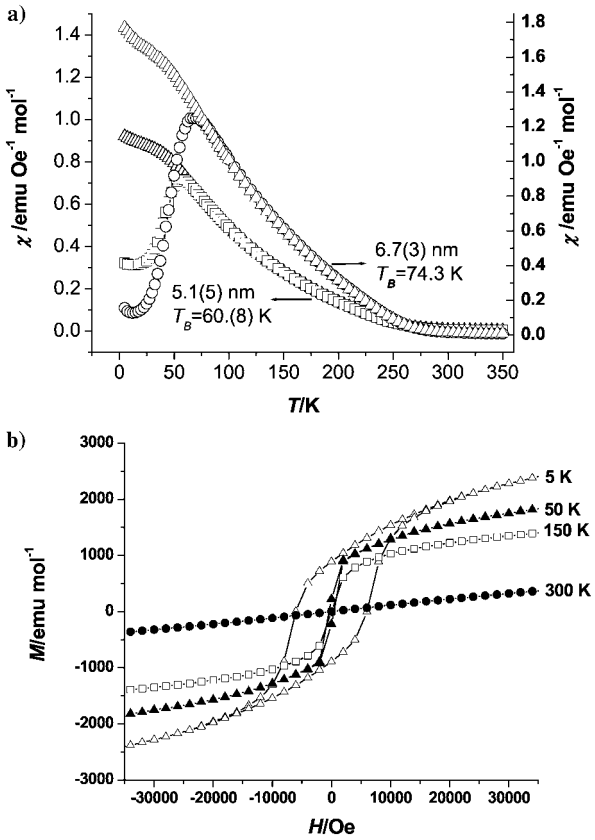

Figure 4. a) Temperature dependence of the magnetization for field cooled (circles and squares) and zero-field-cooled (triangles) MnP nanoparticles under an applied magnetic field of 500 Oe. b) Corresponding variation of magnetization as a function of field for the 5.1(5) nm particles at various temperatures. Reproduced with permission from *J. Am. Chem. Soc.* **2003**, *125*, 13960–13961. Copyright 2003 Am. Chem. Soc.

nanoparticulate MnP is ferromagnetic at all temperatures less than T_c (Figure 4). Also apparent for nanoparticulate MnP is a temperature-dependent transition to a superparamagnetic state (T_B). Between T_c and T_B (the blocking temperature), there is no hysteresis in the magnetization versus field data (i.e., no coercivity) due to thermal fluctuations of the magnetic spin. However, upon cooling below T_B the MnP nanoparticles become coercive, as they are no longer able to fluctuate on the timescale of the measurement (Figure 4b). As expected, the blocking temperature is dependent on crystallite size, with larger crystallites demonstrating higher blocking temperatures than smaller ones, due to the fact that they are more stable to thermal fluctuations (Figure 4). Thus, in contrast to bulk MnP, which loses its ferromagnetism below 50 K, nanoparticulate MnP remains a robust magnet with coercivities of several thousand oersted.

Based on this study, we conclude that FeP nanoparticles are not likely to be responsible for the soft-ferromagnetism observed in Ferrophos alloys, but that nanoparticulate MnP can give rise to ferromagnetic exchange at temperatures below the helimagnetic transition, thus complicating magnetic interpretation of Mn-doped diluted magnetic semiconductors. Finally, we suspect the behavior observed for nanoscale MnP and FeP is likely to be characteristic of other helimagnetic phases that adopt the MnP structure-type (e.g., CrAs),[32] a subject that we will continue to investigate.

Supported Transition-Metal Phosphide Nanoparticles

Impregnation methods: The interest in supported transition-metal phosphides has been driven by their function as heterogeneous catalysts,[33] with the most recent attention on their activity as hydrotreatment catalysts. This area has been recently reviewed,[34] so only an outline will be presented here. The traditional method of preparation is based on impregnation, in which a solid support (typically silica or alumina) is treated with a liquid phase containing the catalyst precursor, followed by annealing. In the case of transition-metal phosphides, the precursors are solutions of metal phosphate, which are evaporated to dryness in the presence of the support. Upon reductive annealing, the dispersed phosphate phase undergoes transformation to transition-metal phosphide nanoparticles, the active catalyst.[35] Hydrotreatment activity has been studied for metal-rich phosphides, including MoP,[36] WP,[37] Ni_2P,[38,39] Fe_2P,[38] and CoP,[38] as both supported and bulk phases. Not surprisingly, supported materials have higher activities, attributed to the greater surface area of nanoparticles (sizes range from ca. 5 nm to 30 nm) relative to the bulk. Among supported cata-

lysts, Ni_2P is (to date) the most effective catalyst for both hydrodenitrogenation and hydrodesulfurization, and is even more active than commercial sulfide-based catalysts.[34]

Organometallic methods: In addition to impregnation, organometallic methods have also been applied to form transition-metal phosphide nanocomposites with silica. Lukehart and co-workers reported that trialkoxysilane-functionalized transition-metal phosphine complexes could be cross-linked with silica sol to form molecularly doped xerogels, which, upon annealing, spontaneously resulted in formation of transition-metal phosphide nanoparticles within the matrix.[40] This method was reported for Fe_2P, RuP, Co_2P, Rh_2P, Ni_2P, Pd_4P_2, and PtP_2 in silica, producing particles with an average size that ranged from 2 to 35 nm, depending on phase. As for the phosphate reduction method outlined above, this method produces single-phase phosphides, and the authors noted that the composition formed was usually that of the congruently melting phase with the greatest phosphorus content. Although an elegant method for composite formation, these materials may be less desirable as catalysts, since the particles form within the matrix and may therefore have fewer accessible catalytic sites.

Using a similar approach, nanoparticles of Co_2P have been produced within the pores of a mesoporous silica.[41] This was achieved by grafting a bis(phosphane)-terminated ligand to the surface and then using this to anchor a zerovalent cobalt carbonyl cluster. Upon annealing, crystalline Co_2P nanoparticles (ca. 60 nm) were observed to form in the pores. A comparative study with a silica xerogel resulted in particles of approximately 200 nm and a broader size distribution, suggesting that the pores were acting to control the particle growth, as well as the spatial arrangement.

Getting a handle on particle size control—nanoparticle precursors for supported phosphides: One issue with all of the supported transition-metal phosphide materials produced to date is the poor control of particle size and polydispersity in the final material. We reasoned that the most rational way to tune the particle size of the phosphide would be to find a way to control the particle size of the phosphate precursor. Our initial work in this area has focused on the preparation of discrete, nanoparticulate iron phosphates and their transformation to iron phosphides.

Iron phosphate precursor nanoparticles were synthesized by modification of a method reported for $LaPO_4$.[42] Thus, refluxing of $FeCl_3$ with crystalline phosphoric acid in a coordinating solvent (tris-2-ethylhexylphosphonate) in the presence of base resulted in formation of an amorphous, colloidal phosphate that could be isolated as a yellow powder by precipitation with methanol. AFM analysis of nanocrystals dispersed on mica suggests the particles are produced in a size range of 2.2 ± 1.2 nm. If this sample is subsequently annealed in a hydrogen-rich atmosphere, the particles become sintered to the mica substrate, and their size decreases to 1.4 ± 0.5 nm, consistent with transformation of phosphate nanoparticles to a phosphide (volume reduction ~75%, Figure 5). This data, in combination with XPS data that confirm the presence of reduced phosphide in the particles, suggests this approach is appropriate for production of supported transition-metal phosphide nanoparticles with modest polydispersities.

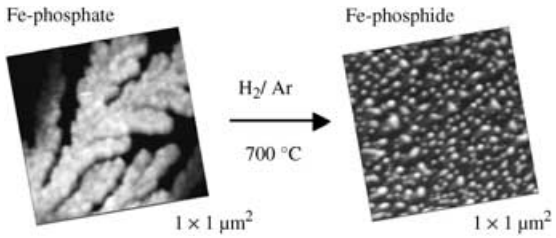

Figure 5. Scheme illustrating the transformation of iron phosphate nanoparticles dispersed on mica to iron phosphide nanoparticles upon reductive annealing (AFM topographic images). Reproduced with permission from *J. Am. Chem. Soc.* **2003**, *125*, 4038–4039. Copyright 2003 Am. Chem. Soc.

Although we have shown that we can directly transform phosphate particles to phosphides, this is only effective when the particles are sufficiently diluted or dispersed. Thus, when the bulk nanoparticulate precipitate is reduced, sintering occurs prior to reduction, resulting in highly crystalline phases, with FeP forming at 700 °C, and transforming to Fe_2P by 1100 °C (Figure 6). Sintering is also evident when

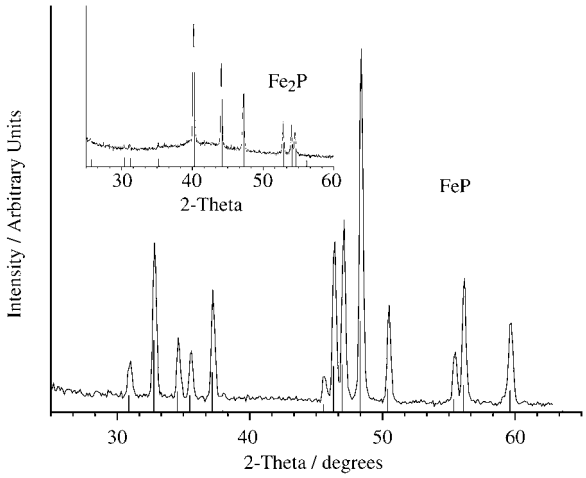

Figure 6. X-ray diffraction patterns of precipitated iron phosphate nanoparticles annealed under H_2/Ar at 700 °C and 1100 °C (inset), and corresponding line diagrams for FeP (JCPDS: 78-1443) and Fe_2P (JCPDS: 85-1725). Reproduced with permission from *J. Am. Chem. Soc.* **2003**, *125*, 4038–4039. Copyright 2003 Am. Chem. Soc.

large quantities of precursor nanoparticles are loaded on the mica substrate. As illustrated in Figure 7, when the initial coverage is relatively high, aggregation occurs, resulting in larger, less uniform particles.

Consequently, this precursor approach, if applied to a high surface-area substrate may produce supported particles far smaller than those achieved by incipient wetness, and with a smaller polydispersity, although whether these materials will be more catalytically active than current materials remains to be seen. Our current focus is on demonstrating the generality of the method for other systems, particularly

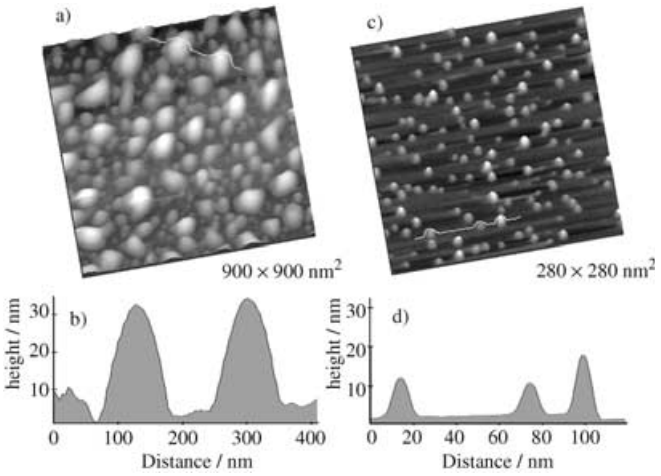

Figure 7. AFM topographic study of iron phosphide nanoparticles after annealing. Surface-confined phosphate precursors were calcined at 700 °C for one hour, in 7% hydrogen in nitrogen. a) Precursor concentration: 2.3 mg mL^{-1}. b) Cursor profile from a). c) Precursor concentration: 0.19 mg mL^{-1}. d) Cursor profile from b). Reproduced with permission from *J. Am. Chem. Soc.* **2003**, *125*, 4038–4039. Copyright 2003 Am. Chem. Soc.

those that would be expected to be more catalytically active (e.g., Ni_2P, MoP).

Conclusion

Although remarkable progress has been made over the last few years on developing new methodologies for preparation of nanoparticles (in general) and transition-metal phosphide nanoparticles (in particular), our synthetic toolbox is still very limited. Furthermore, there is no one-size-fits-all approach that can be applied to main-group and transition-metal phosphides. Thus, desilylation strategies are successful for FeP and InP nanoparticle production, but not MnP; phosphate reduction is effective for preparing supported Ni_2P and MoP, but not main-group phosphides (i.e., GaP, InP).[35] Studies to date on the influence of particle size on magnetic and/or catalytic properties are very provocative and provide an impetus for the development of new synthetic methodologies that will permit control of phase, particle size, particle shape, and sample polydispersity. Additional opportunities in the synthesis of transition-metal phosphide nanoparticles include developing new methodologies (or extending old ones) to target early transition-metal phosphides and more complex compositions (ternary, quaternaries). Finally, there are plenty of opportunities among the heavier pnictides (arsenides, antimonides), which have been even less studied than the phosphides.[43–47]

Acknowledgements

Acknowledgements are made to the donors of the Petroleum Research Fund, administered by the ACS, the National Science Foundation (CAREER award DMR-0094273 and IGERT-970952), and the Institute for Manufacturing Research at Wayne State University for support of this research.

[1] M. Rajamathi, R. Seshadri, *Curr. Opin. Solid State Mater. Sci.* **2002**, *6*, 337–345.
[2] X. F. Qian, Y. Xie, Y. T. Qian, X. M. Zhang, W. Z. Wang, L. Yang, *Mater. Sci. Eng. B* **1997**, *49*, 135–137.
[3] X. F. Qian, X. M. Zhang, C. Wang, W. Z. Wang, Y. T. Qian, *Mater. Res. Bull.* **1998**, *33*, 669–672.
[4] G. Yunle, G. Fan, Y. Qian, Z. Huagui, Y. Ziping, *Mater. Res. Bull.* **2002**, *37*, 1101–1105.
[5] Y. Xie, H. L. Su, X. F. Qian, X. M. Liu, Y. T. Qian, *J. Solid State Chem.* **2000**, *149*, 88–91.
[6] H. L. Su, Y. Xie, B. Li, X. M. Liu, Y. T. Qian, *Solid State Ionics* **1999**, *122*, 157–160.
[7] J. Liu, X. Chen, M. Shao, C. An, W. Yu, Y. Qian, *J. Cryst. Growth* **2003**, *252*, 297–301.
[8] N. Berntsen, T. Gutjahr, L. Loeffler, J. R. Gomm, R. Seshadri, W. Tremel, *Chem. Mater.* **2003**, *15*, 4498–4502.
[9] C. Bao, M. Jin, R. Lu, P. Xue, Q. Zhang, D. Wang, Y. Zhao, *J. Solid State Chem.* **2003**, *175*, 322–327.
[10] D. Battaglia, X. Peng, *Nano Lett.* **2002**, *2*, 1027–1030.
[11] A. A. Guzelian, U. Banin, J. C. Lee, A. P. Alivisatos, *Adv. Met. Semicond. Clusters* **1998**, *4*, 1–34.
[12] H. Yu, J. Li, R. A. Loomis, L.-W. Wang, W. E. Buhro, *Nat. Mater.* **2003**, *2*, 517–520.
[13] S. P. Ahrenkiel, O. I. Miæiæ, A. Miedaner, C. J. Curtis, J. M. Nedeljkovic, A. J. Nozik, *Nano Lett.* **2003**, *3*, 833–837.
[14] Y.-H. Kim, Y.-w. Jun, B.-H. Jun, S.-M. Lee, J. Cheon, *J. Am. Chem. Soc.* **2002**, *124*, 13656–13657.
[15] A. A. Guzelian, J. E. B. Katari, A. V. Kadavanich, U. Banin, K. Hamad, E. Juban, A. P. Alivisatos, R. H. Wolters, C. C. Arnold, J. R. Heath, *J. Phys. Chem.* **1996**, *100*, 7212–7219.
[16] O. I. Mićić, R. J. Sprague, C. J. Curtis, K. M. Jones, J. L. Machol, A. J. Nozik, *J. Phys. Chem.* **1994**, *98*, 4966–4968.
[17] O. I. Mićić, R. J. Sprague, C. J. Curtis, K. M. Jones, J. L. Machol, A. J. Nozik, H. Giessen, B. Fluegel, G. Mohas, N. Peyghambarian, *J. Phys. Chem.* **1995**, *99*, 7757–7759.
[18] X. Peng, J. Wickham, A. P. Alivisatos, *J. Am. Chem. Soc.* **1998**, *120*, 5343–5344.
[19] S. K. Zećević, J. B. Zotović, S. L. Gojković, V. Radmilović, *J. Electroanal. Chem.* **1998**, *448*, 245–252.
[20] B. Cockayne, W. R. MacEwan, I. R. Harris, N. A. Smith, *J. Cryst. Growth* **1985**, *73*, 637–640.
[21] K. Hirose, G. A. Medvedkin, T. Ishibashi, T. Nishi, K. Sato, *J. Cryst. Growth* **2002**, *237–237*, 1370–1373.
[22] K. Sato, G. A. Medvedkin, T. Ishibashi, *J. Cryst. Growth* **2002**, *237–239*, 1363–1369.
[23] K. Sato, G. A. Medvedkin, T. Nishi, Y. Hasegawa, R. Misawa, K. Hirose, T. Ishibashi, *J. Appl. Phys.* **2001**, *89*, 7027–7029.
[24] S. C. Perera, S. L. Brock, *Mater. Res. Soc. Symp. Proc.* **2003**, *455*, DD5.9.1–DD5.9.6.
[25] S. C. Perera, P. S. Fodor, G. Tsoi, L. Wenger, S. L. Brock, *Chem. Mater.* **2003**, *15*, 4034–4038.
[26] S. C. Perera, G. Tsoi, L. E. Wenger, S. L. Brock, *J. Am. Chem. Soc.* **2003**, *125*, 13960–13961.
[27] F. Hulliger, *Struct. Bonding* **1968**, *4*, 83–85.
[28] D. Bellavance, M. Vlasse, B. Morris, A. Wold, *J. Solid State Chem.* **1969**, *1*, 82–87.
[29] G. P. Felcher, F. A. Smith, D. Bellavance, A. Wold, *Phys. Rev.* **1971**, *3*, 3046–3052.
[30] E. E. Huber, Jr., D. H. Ridgley, *Phys. Rev.* **1964**, *135*, A1033–A1040.
[31] G. P. Felcher, *J. Appl. Phys.* **1966**, *37*, 1056–1058.
[32] A. Kallel, H. Boller, E. F. Bertaut, *J. Phys. Chem. Solids* **1974**, *35*, 1139–1152.
[33] E. L. Muetterties, J. C. Sauer, *J. Am. Chem. Soc.* **1974**, *96*, 3410–3415.
[34] S. T. Oyama, *J. Catal.* **2003**, *216*, 343–352.
[35] S. Pandey, K. K. Rangan, J. Gopalakrishnan, *Chem. Mater.* **1997**, *9*, 2113–2116.
[36] D. C. Phillips, S. J. Sawhill, R. Self, M. E. Bussell, *J. Catal.* **2002**, *207*, 266–273.
[37] P. Clark, W. Li, S. T. Oyama, *J. Catal.* **2001**, *200*, 140–147.
[38] X. Wang, P. Clark, S. T. Oyama, *J. Catal.* **2002**, *208*, 321–331.

[39] S. J. Sawhill, D. C. Phillips, M. E. Bussell, *J. Catal.* **2003**, *215*, 208–219.
[40] C. M. Lukehart, S. B. Milne, S. R. Stock, *Chem. Mater.* **1998**, *10*, 903–908.
[41] F. Schweyer-Tihay, P. Braunstein, C. Estournés, J. L. Guille, B. Lebeau, J.-L. Paillaud, M. Richard-Plouet, J. Rosé, *Chem. Mater.* **2003**, *15*, 57–62.
[42] K. Riwotzki, H. Meyssamy, A. Kornowski, M. Haase, *J. Phys. Chem. B* **2000**, *104*, 2824–2828.
[43] J. Lu, Y. Xie, X. Jiang, W. He, G. Du, *J. Mater. Chem.* **2001**, *11*, 3281–3284.
[44] C. Wang, X. F. Qian, X. M. Zhang, Y. D. Li, Y. Xie, Y. T. Qian, *Mater. Res. Bull.* **1999**, *34*, 1129–1133.
[45] Y. Xie, J. Lu, P. Yan, X. Jiang, Y. Qian, *Chem. Lett.* **2000**, 114–115.
[46] X. M. Zhang, C. Wang, X. F. Qian, Y. Xie, Y. T. Qian, *J. Solid State Chem.* **1999**, *144*, 237–239.
[47] Y. Xie, J. Lu, P. Wan, X. Jiang, Y. Qian, *J. Solid State Chem.* **2000**, *155*, 42–45.
[48] K. Selte, A. Kjekshus, *Acta. Chem. Scand.* **1972**, *26*, 1276–1277.

Published online: March 9, 2004

